Structural Engineering and Mechanics, Vol. 24, No. 3 (2006) 355-374 355
DOI: http://dx.doi.org/10.12989/sem.2006.24.3.355

Cellular and corrugated cross-sectioned thin-walled steel bridge-piers/columns

Alper Ucak† and Panos Tsopelas‡

Department of Civil Engineering, Catholic University of America, Washington, DC, USA

(Received August 2, 2005, Accepted April 4, 2006)

Abstract. Thin walled steel bridge-piers/columns are vulnerable to damage, when subjected to earthquake excitations. Local buckling, global buckling or interaction between local and global buckling usually is the cause of this damage, which results in significant strength reduction of the member. In this study new innovative design concepts, "thin-walled corrugated steel columns" and 'thin-walled cellular steel columns" are presented, which allow the column to undergo large plastic deformations without significant strength reduction; hence dissipate energy under cyclic loading. It is shown that, compared with the conventional designs, circular and stiffened box sections, these new innovative concepts might results in cost-effective designs, with improved buckling and ductility properties. Using a finite element model, that takes the non-linear material properties into consideration, it is shown that the corrugations will act like longitudinal stiffeners that are supporting each other, thus improving the buckling behavior and allowing for reduction of the overall wall thickness of the column.

Keywords: bridge pier; cyclic loading; seismic behavior; cellular columns; corrugated columns; pier ductility; pier strength.

1. Introduction

Thin walled steel columns, with either rectangular or circular cross-sections, are commonly used as piers in wind turbines and in elevated highway bridges. Because of their high stiffness to cross sectional area ratio thin walled steel piers are preferred by many engineers over their reinforced concrete counterparts, especially in areas where construction space is limited. After the 1995 Hyogo-ken-Nambu (Kobe) earthquake engineers realized that these structures are vulnerable to damage when subjected to strong cyclic lateral loading. Reconnaissance teams, Chung *et al.* (1996) and Bruneau *et al.* (1996), reported that many steel bridge piers suffered from permanent deformation due to inelastic material behavior and severe local buckling. These irreversible damage patterns are characteristic of thin walled steel sections. Although, many researchers (Kawashima *et al.* 1992, Usami *et al.* 1992) mainly in Japan, had studied the cyclic behavior of thin-walled steel sections before the 1995 Hyogoken-Nanbu earthquake, the research community realized that ductility of those sections was limited by buckling behavior, after that event. As a result, a number of experimental and analytical studies were conducted to determine the factors which could improve ductile behavior under combined axial and horizontal cyclic loading.

† Graduate Student
‡ Associate Professor, Corresponding author, E-mail: TSOPELAS@cua.edu

MacRae and Kawashima (2001) presented experimental results on thin-walled box shape vertically stiffened hollow, as well as, concrete filled steel bridge piers. They reported that local buckling and/or global/wall buckling depended on the flexural rigidity of the vertical stiffeners among other parameters. They also concluded that concrete infill, while it resulted in strength increase, it decreased the deformation capacity. The ductility was also affected by the slenderness of the specimens. Usami *et al.* (1992) presented experimental findings on vertically stiffened hollow and concrete filled steel bridge piers. Their findings included that no significant improvement was observed on ductility, energy absorption capacity, and strength for large changes in the rigidity of the vertical stiffeners, when the rigidity of the vertical stiffeners is beyond a certain threshold. For the concrete filled specimens they observed that they experience significant increase in both the ductility and absorption capacity.

Usami and Ge (1998) conducted an extensive numerical study to determine the factors effecting the ultimate strength and ductility of un-stiffened, vertically stiffened rectangular, and circular steel cross-sections. Gao *et al.* (1998a) performed Finite Element (FE) Analysis studies on short cylinders in compression and flexure to determine the damage potential and ductility capacity of pipe section bridge piers. They found that the ductility of the cylinders is very sensitive to the normalized radius to thickness ratio parameter (R_T), when R_T is smaller than 0.1 (see Eq. (7) in the sequel). The other important finding of this study was that the geometry of the initial deformation of the cylinder along the vertical direction has a significant effect on the ultimate strength and the post-buckling behavior of the pier, while the initial deformations in the circumferential direction have a negligible effect. Gao *et al.* (1998b) through another numerical study reported that both strength and ductility are improved with decrease in R_T and slenderness ratio parameter ($\bar{\lambda}$). Nishikawa *et al.* (1998) conducted experimental studies to investigate the effectiveness of different seismic retrofit schemes for vertically stiffened rectangular and circular cross-sections, which did not include concrete filling. The retrofit schemes involved strengthening the corners of the sides of the rectangular cross sections with inner and outer angle plates and inner flat corner plates. For the circular cross sections they introduced an outer pipe with various clearances from the original circular cross section. For all the retrofit schemes they found that both strength and ductility was improved.

This paper introduces two innovative concepts, thin-walled corrugated cross sectioned steel columns and thin-walled cellular cross sectioned steel columns, in an attempt to improve the strength and ductility capacities of conventional thin-walled steel columns. This is accomplished by eliminating some of the factors which have been identified in the literature as responsible for low ductility performance of thin-walled rectangular and thin-walled circular cross sectioned bridge piers. In doing so, these innovative concepts are taking advantage of the geometry of a cross section. Primarily, those concepts are to be used, but not limited to, in highway bridges as an alternative design or retrofit technique to conventional thin-walled steel piers with circular or rectangular cross-sections. Utilizing a detailed FE model, which takes into consideration both material and geometric nonlinearities, it is shown that the corrugations are acting like longitudinal stiffeners that are supporting each other. This behavior results in improved buckling performance under combined axial and flexural loading, and in a significant increase of both strength and ductility of the piers. First FE models of a circular and a stiffened box thin-walled steel pier are analyzed under cyclic horizontal loading and the results are compared with experimental results available in the literature (Nishikawa *et al.* 1998). Then the calibrated material models are employed to analyze developed designs of cellular and corrugated thin-walled piers and compare their behavior with the behavior of box stiffened and circular cross sectioned piers.

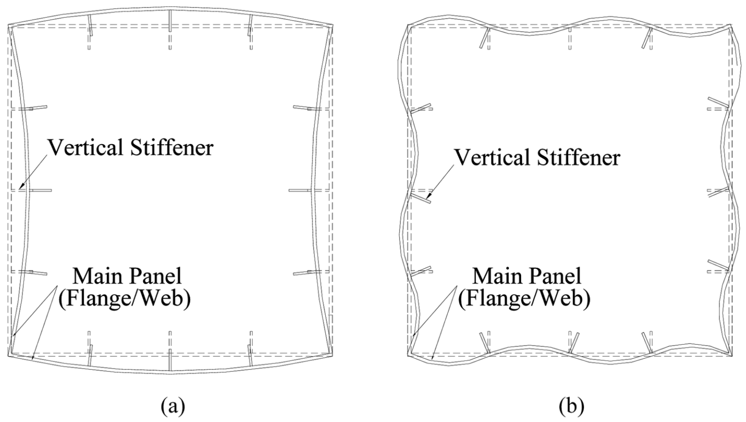

Fig. 1 Typical buckling modes in box section thin-walled columns; (a) wall buckling, (b) panel buckling

2. Buckling of conventional thin-walled steel columns

2.1 Rectangular/box cross sectioned columns

The lateral load capacity and ductility of thin walled columns of rectangular cross section with vertical stiffeners is greatly influenced by the occurrence of buckling. Buckling in turn is affected by the geometry of the cross-section, the boundary conditions of the constituent members of the cross section, the material properties, and the axial load of the column. In stiffened thin-walled rectangular cross sectioned columns two fundamental buckling modes can be identified. These modes are a) wall buckling, where the entire width of the flange and/or the web of the cross section undergo buckling as shown in Fig. 1(a), and b) panel buckling, where the sections of the flange or the web between two successive vertical stiffeners are buckling as shown in Fig. 1(b). Of course a combination of the two fundamental models might exist. In addition it should also be noted that there is an additional possibility, buckling of the vertical stiffeners. Buckling of the vertical stiffeners alone might not directly contribute much to the reduction of the overall strength and ductility of the cross-section. However, buckling of the vertical stiffeners could directly trigger one or a combination of the two aforementioned fundamental buckling modes resulting in low overall strength and ductility of the cross-section.

2.2 Panel and wall buckling

Besides the slenderness ratio parameter ($\bar{\lambda}$) ($\bar{\lambda} = \frac{2h}{r_g}\frac{1}{\pi}\sqrt{\frac{\sigma_y}{E}}$, h is the height of the pier, and r_g is the radius of gyration) of the pier, the mode of buckling and its severity is controlled by two inherent parameters, the normalized plate slenderness ratio (R_R) for panel buckling and the normalized stiffened plate slenderness ratio (R_F) for wall buckling. These parameters are defined according to elastic plate buckling theory as

$$R_R = \sqrt{\frac{\sigma_y}{\sigma_{cr}}} = \frac{B}{nt}\sqrt{\frac{12(1-\nu^2)}{k_r\pi^2}}\sqrt{\frac{\sigma_y}{E}} \tag{1}$$

$$R_F = \sqrt{\frac{\sigma_y}{\sigma_{cr}}} = \frac{B}{t}\sqrt{\frac{12(1-\nu^2)}{k_f\pi^2}}\sqrt{\frac{\sigma_y}{E}} \tag{2}$$

where, E and ν are the Young's modulus and Poisson's ratio respectively; σ_y is the yield stress; σ_{cr} is the critical buckling stress as calculated from the elastic plate buckling theory; B is the width of the side of the rectangular cross section; t is the thickness of the plate; and n is the number of panels separated by vertical stiffeners. The buckling coefficients, which account for the boundary conditions, k_r and k_f are defined as:

$$k_r = 4 \quad \text{(assuming simply supported edges)} \tag{3a}$$

$$k_f = \begin{cases} \dfrac{(1+\alpha^2)^2 + n\gamma_l}{\alpha^2(1+n\delta_l)}; & \alpha < \alpha_0 \\ \dfrac{2(1+\sqrt{1+n\gamma_l})}{1+n\delta_l}; & \alpha > \alpha_0 \end{cases} \tag{3b}$$

where; α is the aspect ratio (a/B) with a being the vertical distance between horizontal stiffeners; δ_l is the ratio of one longitudinal stiffener cross-sectional area to the cross-sectional area of the wall (flange/side of the cross section) ($b_s t_s/Bt$) with b_s and t_s the width and thickness of a stiffener respectively. The relative flexural rigidity of the vertical stiffener with respect to the flexural rigidity of the side of the cross-section (γ_l) and the critical aspect ratio (α_0) are defined respectively as:

$$\gamma_l = \frac{11 I_l}{Bt^3} \tag{4}$$

$$\alpha_0 = \sqrt[4]{1+n\gamma_l} \tag{5}$$

where, I_l is the second moment of inertia of one stiffener calculated with respect to the main panel $(b_s^3 t_s/3)$.

Panel buckling, which is controlled by R_R, will occur when the stiffness of the vertical stiffeners is enough to provide support at the intersections of the wall and the stiffeners (nodal lines). In this case, the panels buckle as multiple half sine waves between the stiffeners with wavelengths equal or smaller to the distance between vertical stiffeners. When the stiffeners cannot prevent horizontal (out of plane) deformations of the panel (see Fig. 1b) at the nodal lines, wall buckling will become dominant, which is controlled by the parameter R_F. It is apparent then, that the strength and ductility of a rectangular cross section of a thin-walled steel pier/column will be controlled by panel buckling when $R_R > R_F$, and wall buckling otherwise.

Since the normalized stiffened panel slenderness ratio takes into account the flexural rigidity of vertical stiffeners, an optimum value of the flexural rigidity for the vertical stiffeners (γ_l^*) can be obtained by equating Eq. (1) and Eq. (2), such that wall buckling and panel buckling occur simultaneously. Using γ_l^* the mode of buckling can be identified from the ratio γ_l/γ_l^*, which is the ratio of the relative flexural rigidity of the vertical stiffeners to its optimum value. Thus panel buckling will occur when the flexural rigidity of the stiffeners is grater than the optimum flexural rigidity of the stiffeners, i.e., $\gamma_l/\gamma_l^* > 1$, and wall buckling will occur otherwise. The interested reader can find additional information on γ_l, and γ_l^* in MacRae and Kawashima (2001), Uang *et al.* (2000) and Kristek and Skaloud (1991).

2.3 Vertical stiffener buckling

The validity of the aforementioned panel and wall buckling equations (Eq. (1) and Eq. (2)) are limited to general instability of the plate between the stiffeners and the stiffened wall as a whole excluding effects such as local buckling of the stiffeners, cross-sectional distortions, and shear deformations of the stiffeners, all of which decrease the effective moment of inertia of the stiffener. In order for Eq. (1) and Eq. (2) to be valid, local buckling potential of the vertical stiffeners have to be eliminated. The buckling of the vertical stiffeners is controlled by the slenderness ratio of the flat bar stiffeners, which can be written as:

$$R_s = \sqrt{\frac{\sigma_{ys}}{\sigma_{cr,s}}} = \frac{b_s}{t_s}\sqrt{\frac{12(1-\nu^2)}{k_s\pi^2}}\sqrt{\frac{\sigma_{ys}}{E}} \tag{6}$$

where the buckling coefficient $k_s = 0.43$

From experimental and numerical data available in the literature it is hard to determine limiting values for the width to thickness ratios for the panel (R_R), wall (R_F) and the stiffener (R_S) after which buckling can be prevented so that the cross-section yields and reaches its ultimate capacity before a buckling mode appears. However it can be argued that ultimate strength and ultimate deformation capacities can be increased by decreasing the values of R_R, R_F and R_S. That in turn results in an increase of the safety factor against potential effects from geometrical imperfections, and residual stresses. Hanshin Expressway Public Corporation requires that R_R and R_F to be less than 0.4 and R_S to be less than 0.5 for vertically stiffened rectangular steel piers. Moreover it is suggested that the ductility of a rectangular stiffened cross-section increases with the increase of γ_l/γ_l^*.

2.4 Circular cross sectioned columns

Experimental studies show that the buckled geometry in circular cross-sections has an elephant foot shape and that the buckling is controlled by the normalized radius to thickness ratio parameter of the circular cross-section which is defined according to the elastic buckling theory as

$$R_T = \frac{\sigma_y}{\sigma_{cr}} = \frac{r}{t}\sqrt{3(1-\nu^2)}\frac{\sigma_y}{\sigma_{cr}} \tag{7}$$

where, r is the radius of the cross section, and t is the thickness of the cross-section.

Gao *et al.* (1998a) presented a thorough analytical investigation on the factors that affect ductility and strength of steel cylinders under compressive and bending actions and reported that circular columns with R_T smaller than 0.05 exhibit desirable behavior under lateral cyclic loading. They showed that the lateral load vs deformation loops are stable showing constant strength and increasing energy dissipation capability as the plastic deformations increase. This stable behavior can be attributed to limited local buckling concentrated close to the base of the column. The area that the material has been undergoing buckling with each cycle remains confined and buckling does not propagate to the rest of the column. Failure occurs due to excessive plastic deformations when strain reaches an ultimate value. However, columns with $R_T < 0.05$ are not considered economically

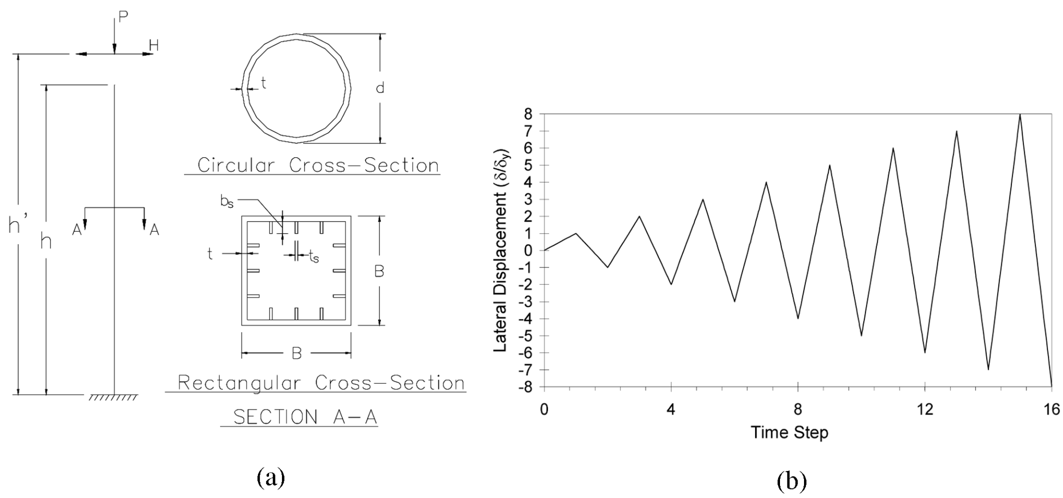

Fig. 2 Cross sections of the tested specimens by Nishikawa *et al.* (1996). The circular cross section is No-8, and the stiffened rectangular cross-section is No-2.

viable solutions to be used in practice. As a result both strength and ductility are limited by buckling in actual bridge pier designs.

2.5 Experimental studies by Nishikawa et al. (1998)

Nishikawa *et al.* (1998) tested 1/3-scale thin walled columns, with circular and rectangular cross-sections, under both axial and cyclic horizontal loading, at the Public Research Work Institute of Japan. A sketch of the test setup and the cyclic loading path are shown in Fig. 2(a) and Fig. 2(b) respectively. The interested reader is referred to Nishikawa *et al.* (1998) and to Goto *et al.* (1998) for details on the prototype design work as well as the geometry and material properties of the two of the tested columns (one circular and one stiffened box section) which were chosen to be analyzed in this study.

Table 1 presents the geometry and the mechanical properties of the stiffened box cross sectioned column (No-2) and the circular cross sectioned column (No-8). FE analysis of the two tested specimens by Nishikawa is carried out to establish reliable geometric and material constitutive models which will be utilized in the study of the proposed cellular and corrugated cross sectioned columns. The location of the application of the loads (axial and horizontal) is at a height (h') from the base of the columns. The diameter of the circular cross sectioned column is indicated by (d) and the side/wall length of box cross sectioned column is depicted by (B). The thickness of the walls is denoted by (t), where the stiffeners thickness and length are indicated by (t_s) and (b_s).

The loading path consists of a cyclic motion of increasing amplitude. Only one cycle is applied at each amplitude, which increases from $\delta = 1\ \delta_y$ to $\delta = 8\ \delta_y$. The lateral displacement amplitude is in terms of a computed value of "yield displacement" of the column (δ_y). This value is calculated using $\delta_y = (H_y h'^3)/(3EI_{zz})$, where, E is the modulus of elasticity of the material, and H_y is given by this expression: $H_y = (\sigma_y - P/A)I_{zz}/(Bh')$.

Table 1 Geometric and mechanical properties of the tested specimens by Nishikawa *et al.* (1998)

Specimen \ Parameter	h' (mm)	B/d (mm)	$t/t_s/b_s$ (mm)	A (mm^2)	I_{zz} (10^9 mm^4)	P (kN)	$P/(\sigma_y A)$	H_y (kN)	δ_y (mm)
No-2 Stiffened Box Section	3403	900	9/6/80	37836	4.80	1747	0.122	1029	13.8
No-8 Circular Cross Section	3403	900	9/-/-	25192	2.50	904	0.124	414.9	10.6

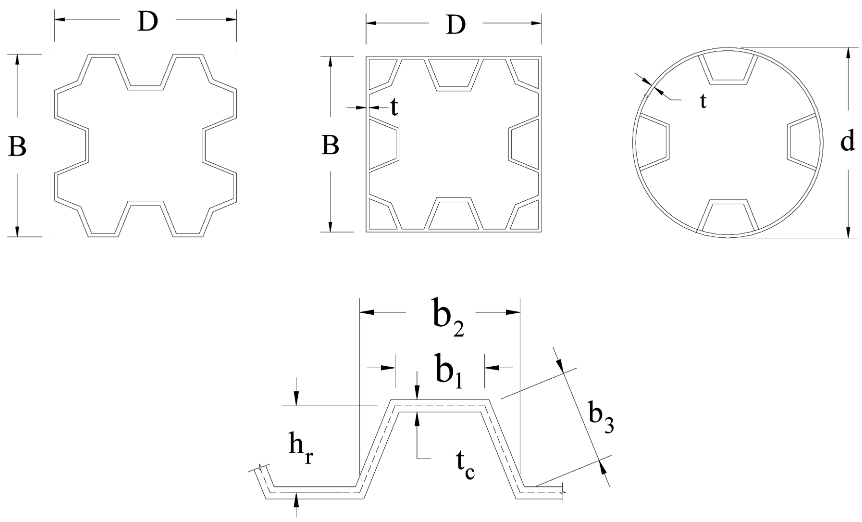

Fig. 3 Corrugated and cellular cross sections with corrugated patterns and details of their geometry (ALT-C-8, ALT-2, and ALT-8)

3. Corrugated and cellular thin-walled steel columns

The shortcomings of the thin-walled rectangular and circular cross-sections, as described previously, are their inability to fully utilize the strength and ductility capacities of the cross sections due to pre-mature buckling behavior (local or global buckling before yielding of the material). In order to overcome these shortcomings a corrugated thin-walled cross-section and two cellular cross sections incorporating corrugated patterns are proposed as alternatives to the conventional thin-walled stiffened box and circular cross sections. A corrugated column consists of either cold-formed corrugated plates or inclined plates that are welded to each other as depicted in Fig. 3. In a corrugated column, each plate or fold is expected to act like a stiffener that supports the adjacent plate in the vertical direction. At the first glance the corrugated column may look similar to a rectangular shaped column with vertical stiffeners. However, since each fold is supported on both vertical edges, the buckling properties of corrugated columns are more desirable than the stiffened rectangular and circular cross sections.

The lateral strength of a corrugated column depends on the critical buckling stress of each corrugation. Each fold or corrugation panel is supported on both sides by neighboring folds which

Table 2 Geometric properties of the alternative designs; cellular and corrugated sections

Specimen \ Parameter	h' (mm)	$B = D/d$ (mm)	t (mm)	t_c (mm)	b_1 (mm)	b_2 (mm)	h_r (mm)
ALT-2 Cellular Box Section with Corrugated Pattern	3403	900	7	7	150	270	147
ALT-8 Circular Cross Section with Cellular Stiffeners	3403	900	7	7	130	195	90
ALT-C-8 Corrugated Cross Section	3403	900	6.35	6.35	150	270	47

are acting as vertical stiffeners. The size, orientation, and boundary conditions of each fold affect their rigidity (each fold has a dual purpose it works both as a stiffener and as part of the cross-section wall) and accordingly reduce the buckling potential of the folds when it is compared to the stiffened box cross sections. In addition, since the corrugation width, which is subjected to buckling, is much smaller than the wall width in rectangular sections, higher critical buckling stresses can be achieved with thinner plates. Moreover, local buckling in a single corrugation will not cause failure because the sharp edges between the folds will prevent buckling from propagating in the neighboring folds and the whole cross-section. As a result the section can undergo large plastic deformations without significant, if any, strength reduction, hence dissipate large amounts of energy under horizontal cyclic loading or seismic excitations.

Furthermore, a corrugation pattern gives design flexibility in the hands of the engineer; by changing the corrugation density the engineer can control the critical buckling stress. With denser corrugations higher critical buckling stresses can be achieved. However, if the corrugations are too dense failure will occur due to global buckling of the compression flange, similar to buckling modes of orthotropic plates and similar to the wall buckling mode of the stiffened rectangular cross section as discussed previously, which is not desirable in this case. For the design of the cellular and the corrugated cross-sectioned columns the same equations and procedure can be used as the one presented previously for the conventional cross section. Eq. (8) presents the corrugated panel/fold slenderness ratio which controls to a large extent the critical buckling strength of the corrugated panels/folds.

$$R_{CP} = \sqrt{\frac{\sigma_y}{\sigma_{cr}}} = \frac{b_1 \text{ or } b_3}{t_c}\sqrt{\frac{12(1-\nu^2)}{k_{CP}\pi^2}}\sqrt{\frac{\sigma_y}{E}} \tag{8}$$

where, k_{CP} is the coefficient that takes into account the boundary conditions of the panel in a similar manner as the corresponding coefficients in Eq. (1), Eq. (2), and Eq. (6). It should be noted here that the boundary conditions are neither simple supports nor fully fixed, but rather somewhere in between those two conditions.

Table 2 and Table 3 present the geometry and the mechanical properties of the two cellular cross sections (ALT-2 and ALT-8) and the corrugated cross section (ALT-C-8).

As can be seen by comparing Tables 1, 2, and 3 all cellular and corrugated cross section designs utilize thinner walls; 7 mm thickness for ALT-2 and ALT-8, and 6.35 mm for ALT-C-8 compared to

Table 3 Mechanical properties of the alternative designs; cellular and corrugated sections

Specimen \ Parameter	A (mm^2)	I_{zz} (10^9 mm^4)	P (kN)	$P/(\sigma_y A)$	H_y (kN)	δ_y (mm)
ALT-2 Cellular Box Section with Corrugated Pattern	44757	5.05	2047	0.122	1085	13.7
ALT-8 Circular Cross Section with Cellular Stiffeners	28204	2.57	1012	0.124	427	10.56
ALT-C-8 Corrugated Cross Section	25846	2.50	905	0.124	414.9	10.6

9 mm wall thickness for the No-2 and No-8 cross sections. The design of the alternative cross sections was such that the overall dimensions, the cross sectional area, and the moment of inertia, the three important parameters which affect the performance of the columns, to be as close as possible to the properties of the conventional cross-sections. To a certain extent that was achieved, especially for the corrugated cross section (ALT-C-8) and the circular cross section (No-8). For the other cases ALT-2 vs No-2 and ALT-8 vs No-8 some minor differences in A and I_{zz} were inevitable, however, in these cases the axial load was adjusted (increased) such that the ratio $P/(\sigma_y A)$ is the same. The values of the H_y and δ_y, which are used to normalize the hysteretic curves, for the cross sections are also very similar.

3.1 Finite element modeling

To determine the hysteretic behavior, FE analyses are carried out which take both material and geometric non-linearities into consideration. For this purpose the commercial multi purpose finite element package ANSYS Ver.8.1 is used. The specimens are modeled using non-linear Shell 181 elements that are available in ANSYS element library. Using symmetric boundary conditions, only half of each column is considered in the analysis. At the base, fixed boundary conditions are applied. The mesh for the circular and rectangular columns is determined using a trial and error approach so that the errors between FEM analysis and test results were minimized. Similar to the results reported by Usami and Ge (1998) it is found that for stiffened rectangular cross-sectioned columns the effect of mesh size becomes negligible when the distance between the base and the first horizontal diaphragm, the region which buckling is expected to occur, is divided into larger than 18 segments and the stiffeners are divided into minimum two horizontal segments. For circular cross-sectioned columns the analysis becomes independent of the mesh size when minimum 40 elements are used to span the lowest section of the column which is located directly above the base and has a height equal to the column diameter. For the cross sections incorporating corrugations a higher mesh density is required as it can be observed in Fig. 4. The mesh density is determined through trial and error; (when the error between two successive analyses for a mesh density increment is negligible then no further mesh increase is applied). It was found that the difference in the hysteretic behavior when each corrugation is divided into three and six elements is negligible small. However, a mesh density where each corrugation is divided into minimum six elements is

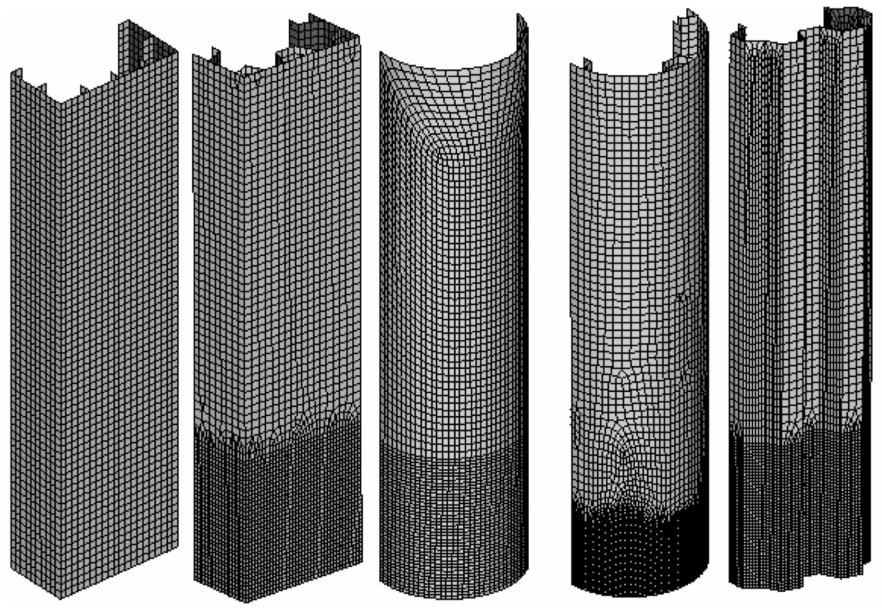

(a) (b) (c) (d) (e)

Fig. 4 Meshed geometries of the FE Models utilized in this study. (a) Stiffened box section column No-2, (b) Cellular boxed section with corrugated pattern ALT-2, (c) Circular cross section No-8, (d) Circular cross section with cellular stiffeners ALT-8, (e) Corrugated cross section ALT-C 8

used through out the study. The final meshed geometries of the analyzed columns are shown in Fig. 4.

Structural steel has a rather complex material behavior. Especially in cyclic-large deflection analyses the accuracy of the results will depend on the ability of the material model to reflect the complex non-linear material behavior. In this study the constitutive model utilized to represent the material behavior of structural steel is the one proposed by Chaboche (Lemaitre and Chaboche 1990) with the non-linear kinematic hardening rule, a von Mises yield criterion and an associative flow rule. The von-Mises yield criterion can be expresses as:

$$f = J_2(\boldsymbol{\sigma} - \mathbf{X}) - k \tag{9}$$

where, J_2 is the second stress invariant, $\boldsymbol{\sigma}$ is the stress tensor, $\mathbf{X}$ is the back stress tensor, k is the yield stress. For the nonlinear kinematic hardening behavior Chaboche proposed that the back stress increment should be written as:

$$d\mathbf{X} = \frac{2}{3}Cd\boldsymbol{\varepsilon}^p - \gamma\mathbf{X}dp \tag{10}$$

where, $d\boldsymbol{\varepsilon}^p$ is the increment of plastic strain tensor, dp is the increment of the accumulative plastic strain and C and γ are the characteristic coefficients of the material (parameters of the model). The interested reader is referred to Lemaitre and Chaboche (1990) for additional details of the plasticity formulation with this nonlinear kinematic hardening rule.

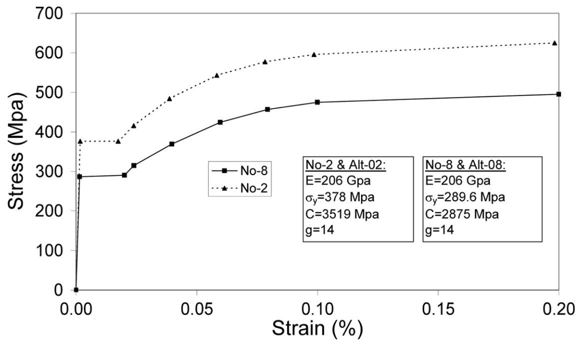

Fig. 5 Material constitutive model utilize in the prediction of experimental results by Nishikawa *et al.* (1998)

Table 4 Chaboche model parameters

	E (GPa)	σ_y (MPa)	C (MPa)	γ
No-2 / ALT-2	206	378	3519	14
No-8 / ALT-8	206	289.6	2875	14

Model parameters are calibrated using the stress-strain curves shown in Fig. 5, which are reported by Nishikawa *et al.* (1998). The constitutive material model parameters are presented in Table 4.

In the present analyses the effects of residual stresses and initial deflections of the column walls are neglected for all the cross-sections. These effects will accelerate some buckling modes (Banno *et al.* 1998), and might affect the cyclic behavior of the specimens to a certain extend. However, since no imperfection measurements were reported in Nishikawa *et al.* (1998) and since this study investigates the global behavior of the corrugated cross sections rather than attempting to provide expressions or equations to be used in the design process, these effects are neglected.

3.2 Comparisons between analytical and experimental results for rectangular and circular cross-sectioned piers

Initially, the force-deformation loops obtained from the FE analyses are compared with the experimental results reported by Nishikawa *et al.* (1998). Since the test results were not available to the authors the experimental force-deformation curves, which are reported here in, are obtained by digitizing the figures in the original publication by Nishikawa *et al.* (1998).

Fig. 6(a) compares the hysteretic loops obtained from the FEM analyses with the ones reported by Nishikawa *et al.* (1998) for the stiffened box cross-sectioned column No-2. In the figures, the shear force of the column (H) is normalized by the yield force (H_y), and the lateral displacement of the column top (δ) is normalized by the yield displacement (δ_y). As can be seen from the force-deformation curve, the FE model predicts the elastic stiffness, the buckling load, as well as the stiffness deterioration and the strength degradation accurately. Fig. 6(b) depicts the deformed shape at the end of the analyses and the deformed shape observed at the end of the experiment as reported in Goto *et al.* (1998). The buckled shape has the appearance of a half sine-wave pointing inward in the flange and outward in web; this shape is captured accurately by the analysis of the developed FE Models.

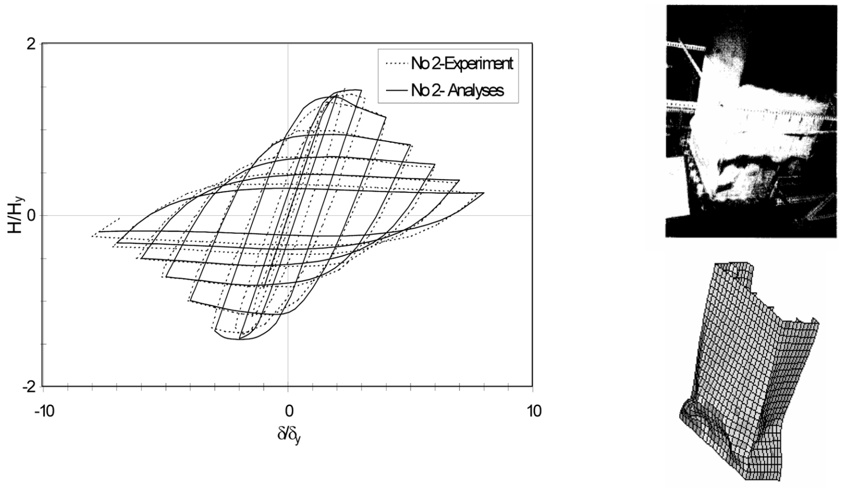

(a) (b)

Fig. 6 Experimental vs FEM analysis results of a stiffened box sectioned column; (a) Normalized shear force vs normalized lateral displacement loops, and (b) final buckled shape adjacent to the base. Experimental results by Nishikawa *et al*. (1998)

The validity of this study depends on the accuracy of the finite element results. For this reason, the analyses results obtained for the stiffened box section is compared with the experimental results and good agreements are obtained. The initial stiffness and the ultimate strength as well as the strength and stiffness degradation obtained from the analyses agreed well with the ones from the experiment. The ultimate capacity of the box section predicted by the analyses F_{ult} = 1530 kN differs only by 2‰ from the experimental results.

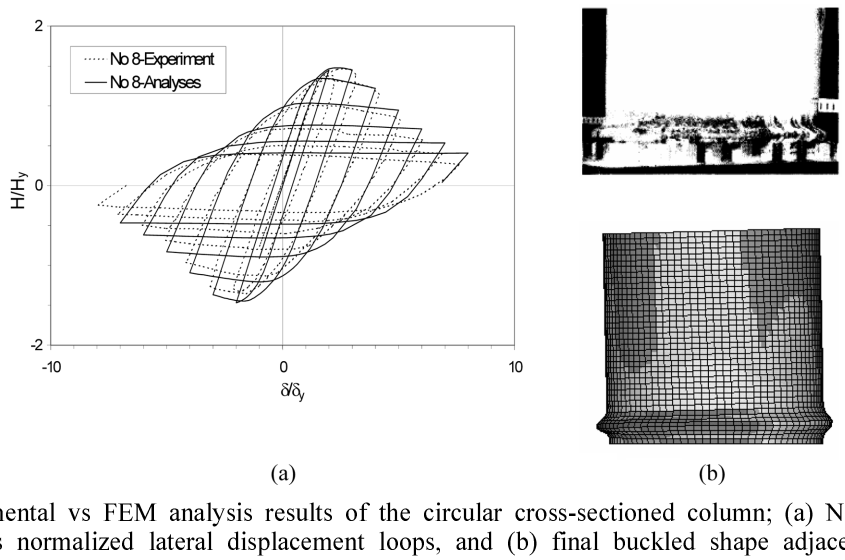

(a) (b)

Fig. 7 Experimental vs FEM analysis results of the circular cross-sectioned column; (a) Normalized shear force vs normalized lateral displacement loops, and (b) final buckled shape adjacent to the base. Experimental results by Nishikawa *et al.* (1998)

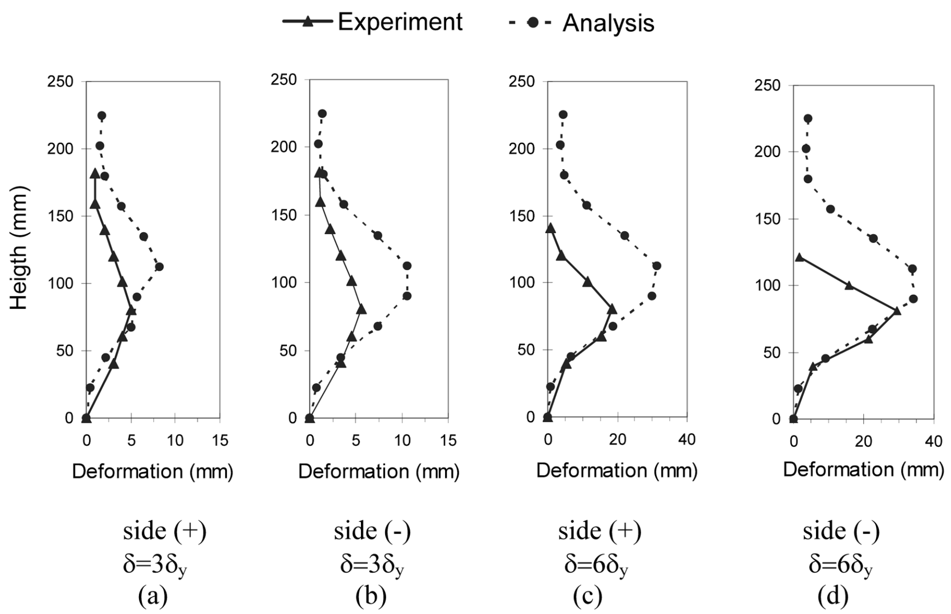

Fig. 8 Experimental vs FEM analysis results of the buckled shape of two sides of a circular cross sectioned column at two levels of lateral deflection; (a) side (+) at $\delta = 3\delta_y$, (b) side (–) at $\delta = 3\delta_y$, (c) side (+) at $\delta = 6\delta_y$, (d) side (–) at $\delta = 6\delta_y$

Fig. 7(a) compares FE analysis results for the circular cross-section column with the experimental results for the same column reported by Nishikawa *et al.* (1998). Comparing their hysteretic behavior in terms of lateral force vs lateral deflections loops it is evident that the FE results are in very good agreement with the experimental results. Slight differences in the elastic stiffness can be attributed to the rigid foundation assumption, which might not have reflected the actual conditions of the column base during the experiment. The finite element model, however, captures the buckling load and the strength degradation rather accurately, except the slight overestimation of the column strength towards the end of the analyses at large lateral displacements.

Fig. 8 presents the deflected shape of the circular cross section close to the base (within a height of 250 mm) of the column at two opposite sides, side plus (+) and side minus (–), at two levels of lateral deflection of the top of the column, $\delta = 3\delta_y$ and $\delta = 6\delta_y$. The experimental results were digitized from the results presented in Goto *et al.* (1998). It can be observed that the computational modeling captures the experimental results relatively well. The tendency in the analytical results for the max lateral deflection at buckling to occur higher than the experimental results can be attributed to the boundary conditions which in experiments were not fixed.

4. Analytical results and disscussion

The previously presented comparisons between experimental and FE analysis results established that the material and geometric models are appropriate to accurately capture the cyclic response of thin-steel cross sectioned columns under lateral loading. Nonlinear behavior, due to material, geometry and large deflections can be modeled correctly. In addition, complicated instability phenomena such as plastic buckling, either local or global, could be simulated with acceptable accuracy. Utilizing the material models used in the previous analysis a computational study is performed to compare the cyclic behavior of the conventional thin-walled steel cross sectioned columns with the cellular and corrugated alternative designs.

4.1 Comparison between stiffened box (No-2) and cellular with corrugated stiffeners (ALT-2) cross sections

The conventional stiffened box cross-sectioned column (No-2) and the cellular boxed section with the corrugated pattern column (ALT-2) were analyzed under the same normal loading conditions, same average compressive stress ($P/(\sigma_y A) = 0.12$), and the same cyclic horizontal displacement (see induced lateral displacement path in Fig. 3(b). As can be observed from Tables 1 and 3, although the cross sectional area of the corrugated column is higher than the box section, their second moment of inertias and the yield displacements are comparable.

Fig. 9 compares the hysteretic behavior of the two models obtained from FE analysis. Since both sections have the same elastic stiffness both sections respond similarly to applied lateral load for the first two cycles ($\delta = 2\delta_y$). In the stiffened box section, buckling occurs when the displacement amplitude is between $2\delta_y$ and $3\delta_y$. At $\delta = +4\delta_y$ the strength of the section has dropped to 74% of its ultimate strength, which was attained during the 3rd cycle. As the displacement amplitude increases the strength of the section continues to decrease rapidly and finally at displacement amplitude equal to $+8\delta_y$, the strength of the pier has been reduced to only 17% of its ultimate strength. It should be noted that the strength drop at $\delta = -4\delta_y$ and $\delta = -8\delta_y$ is significantly more than the aforementioned values. In addition, the hysteretic loops of the stiffened box section show significant stiffness degradation. From 63.95 kN/mm elastic stiffness in the first cycle, to 16.43 kN/mm in the 8th and last cycle, as can be clearly observed from the unloading branches of the force-deformation loops.

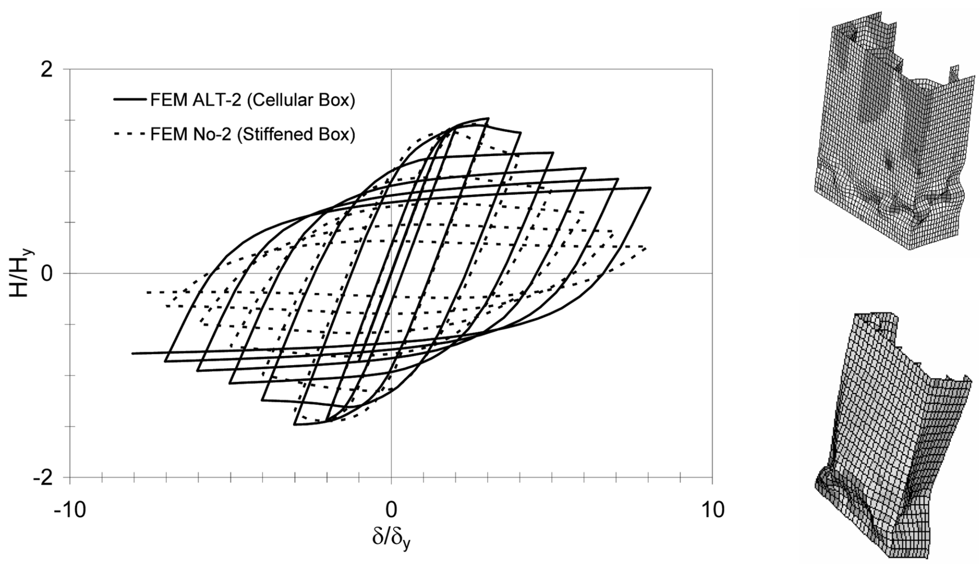

Fig. 9 Hysteretic curves for the No-2 and ALT-2 sections obtained from FE analyses

The stiffness degradation begins at the loading branch corresponding to $-2\delta_y$ displacement, indicating that local buckling initiated at displacement amplitude equal to twice the yield displacement δ_y. Beyond displacement $\delta = 4\delta_y$ the stiffness drops rapidly with the increase of the displacement amplitude, indicating the local buckling has propagated throughout the section and global/wall buckling has occurred. Another way to quantify the stiffness degradation is by looking at the effective stiffness. Effective stiffness is defined as the ratio between max force vs max displacement attained in each cycle, and for the first cycle effective stiffness coincides with the elastic stiffness. The effective stiffness of the box section drops from 63.95 kN/mm in the first cycle to 2.49 kN/mm in the 8th and last cycle.

The column with the cellular cross section with the corrugation pattern on the other hand shows slight strength deterioration, 9% drop from the ultimate strength, at the fourth cycle ($4\delta_y$), which indicates that local buckling initiated between $3\delta_y$ and $4\delta_y$ displacement amplitudes. Beyond this point the strength of the section decreases in a controlled manner resulting to strength levels of the order of 45% of the ultimate at the last cycle (8th cycle). Unlike the box-sections the hysteretic loops of the corrugated section do not show significant stiffness degradation, from 68.37 kN/mm elastic stiffness in the first cycle, to 50.94 kN/mm in the 8th and last cycle, as can be observed from the unloading branches in Fig. 9. Looking at the effective stiffness for the corrugated column the effective stiffness at the 8th cycle is equal to 8.2 kN/mm, which is 4 times higher than the effective stiffness of the box section at the same displacement amplitude. That can be attributed to the rather localized buckling behavior and to a higher post buckling strength of the cellular cross section when it is compared to the stiffened box section.

The deformed shape of the two cross sections at displacement amplitude $\delta = +8\delta_y$ can be observed in Fig. 9. The difference in the failure modes that the two cross-sections experience is apparent, with global/wall buckling dominating the shape of the stiffened box cross section and buckling in the cellular cross section to be confined to a local buckling mode. The corrugations of the cross section are acting as barriers and do not allow local buckling to turn into global/wall buckling which is responsible to the strength and stiffness reductions reported previously.

4.2 Comparison between circular cross sections with (ALT-8) and without (No-8) cellular stiffeners

Fig. 10 presents the shear force vs lateral displacement loops for circular cross sectioned columns with and without cellular stiffeners acquired from FE analysis. Both sections respond similarly to the applied lateral load for the first two cycles ($\delta = 2\delta_y$). However, at displacement $\delta = 3\delta_y$ the circular cross section (No-8) has already reached its peak strength (at $\delta = 2.37\delta_y$) and buckling has started affecting the secant stiffness of the column. It can be clearly observed in Fig. 10 that the secant stiffness takes "negative" values. In contrast, the circular cross section with cellular stiffeners (ALT-8) does not experience any "negative" secant stiffness even when the lateral displacements reached very high values.

At $\delta = +4\delta_y$ the strength of the circular section (No-8) has dropped by 17% compared to the ultimate strength, which was observed at $\delta = 2.37\delta_y$. As the displacement amplitude increases the strength of the circular section continues to decrease and at amplitude equal to $+8\delta_y$, the strength of the pier has been reduced by 72% of its ultimate strength. It should be pointed out here that compared to the stiffened box section, which was discussed previously, the circular cross section seems to be holding better with almost twice the strength remaining at $\delta = 8\delta_y$.

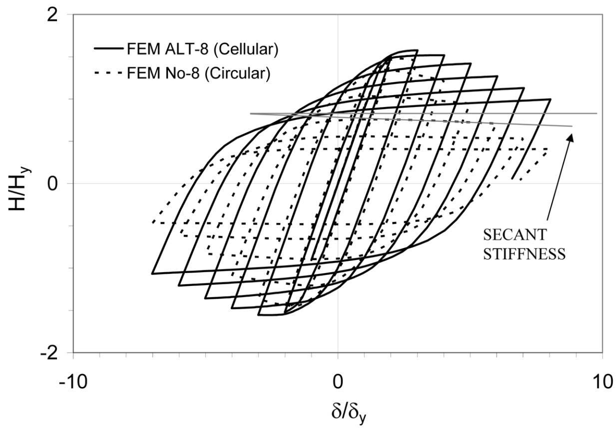

Fig. 10 Hysteretic curves for the No-8 and ALT-8 sections obtained from FE analyses

The column with the cellular cross section (ALT-8) experiences very small strength degradation (3.6% drop from the ultimate strength), at the fourth cycle ($4\delta_y$), which indicates that local buckling has been contained and has not affected the global behavior of the column. After that the strength drops with a rather constant rate and at δ = $8\delta_y$ the remaining strength is 73.2% of its ultimate strength, which is almost twice the remaining strength of the circular cross section (No-8).

To evaluate the stiffness deterioration of each cross section as amplitude increases one has to observe the unloading branch of each hysteretic loop in Fig. 10. The circular cross sectioned column (No 8) has lost 74% of its elastic stiffness at the 8th cycle (dropped from elastic stiffness of 35.7 kN/mm to 12.81 kN/mm). The corresponding stiffness deterioration for the ALT-8 column is 22% at the 8th cycle (from 36.1 kN/mm to 28.17 kN/mm). The effective stiffness of the circular cross section (No 8) drops from 35.7 kN/mm in the first cycle to 2.0 kN/mm in the 8th and last cycle, where for the ALT-8 circular cross section with cellular stiffeners dropped from 36.1 kN/mm to 5 kN/mm.

Fig. 11 presents the deformed shape of the two cross sections at displacement amplitude $\delta = +8\delta_y$. The lateral deformations, bulging, of the ALT-8 cross section close to the base are smaller when compared to the deformations in No-8 cross section at the same cycle (8th). The contribution of the cellular stiffeners in controlling buckling is shown in Fig. 11(c).

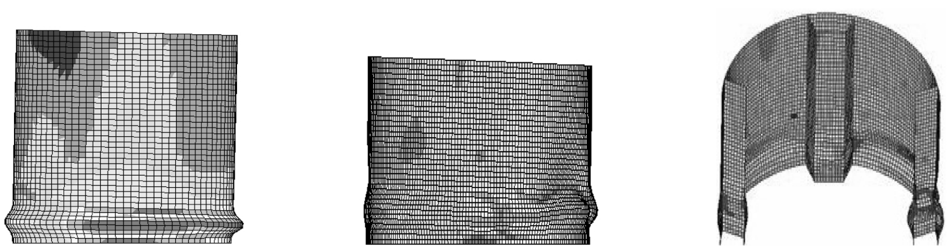

(a) (b) (c)

Fig. 11 Deformed shapes of the lower part of the columns at $\delta = 8\delta_y$ obtained from FEM analysis. (a) outside view of the column with circular cross section (No-8), (b) outside view of the column with the cellular stiffeners (ALT-8), and (c) inside view of the of ALT-8 column

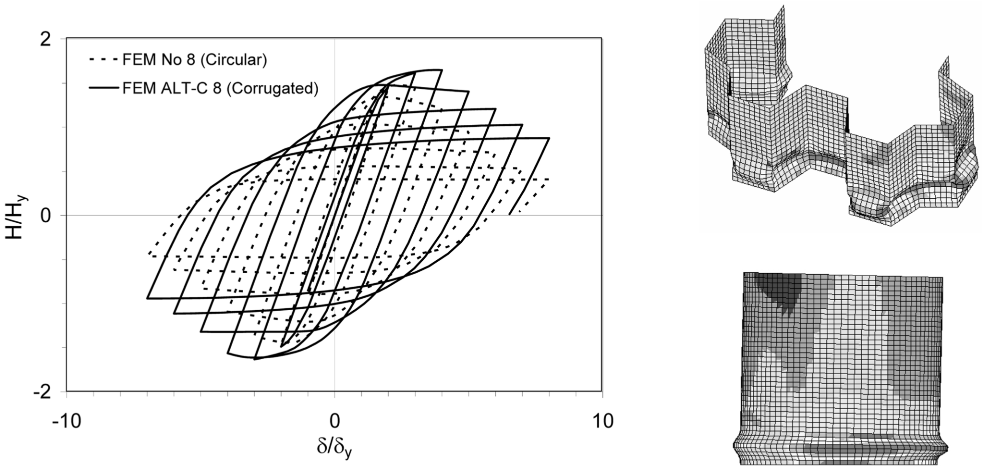

Fig. 12 Hysteretic curves for the No-8 and ALT-C-8 cross sectioned columns and deformed shape of the two columns at $\delta = 8\delta_y$

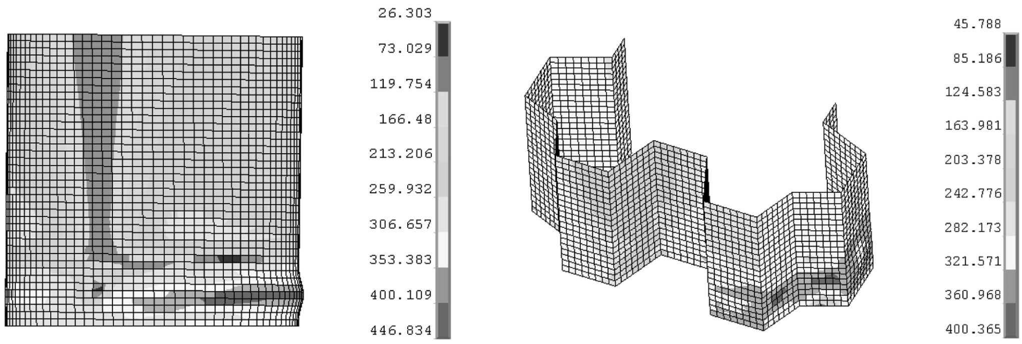

Fig. 13 Von-Misses stress distribution in No-8 and ALT-C-8 columns at lateral deflection $\delta = 4\delta_y$. The stress units in the figures are MPa.

4.3 Comparison between circular cross section (No-8) and corrugated cross section (ALT-C-8)

A corrugated cross section (ALT-C-8) was developed as an alternative to the circular cross sectioned column (No-8). Horizontal force vs lateral displacement loops of the circular cross sectioned column (No-8) and its alternative corrugated cross sectioned column (ALT-C-8) are presented in Fig. 12. The behavior of the corrugated cross section under lateral cyclic loading is superior to the behavior of the No-8 column. As it can be seen from Table 1 and Table 3 the cross sectional area, and the moment of inertia of the two cross sections are nearly identical, however the ultimate strength of the corrugated cross section ($Fu = 684.3$ kN), which is reached at $\delta = 3.8\delta_y$, is 12% higher than the ultimate strength of the No-8 column ($Fu = 612.9$ kN), which is reached at $\delta = 2.37\delta_y$. Once more the rates at which the strength degrades and the stiffness deteriorates for the corrugated cross section are much lower than the same rates for the No-8 pier as becomes evident from Fig. 12. While the strength reduction with respect to the ultimate of the circular cross section at $\delta = 8\delta_y$ is 72% (169.4 kN), the corrugated cross section has lost only 45% (363.1 kN) of its ultimate strength at the same lateral displacement amplitude.

Fig. 13 shows the stress distribution (Von-Misses Stress) in the lower part of the columns at $\delta = 4\delta_y$. It can be observed from the legends that the circular cross section experiences higher stress amplitudes compared to the corrugated cross section. The circular cross section is undergoing significant buckling deformations; in contrast, the corrugated cross section experiences some minor local buckling of one of the folds which is almost indistinguishable from the figure.

4.4 Ductility capacity

Ductility is defined as the ability of a system to withstand large deformations at a relatively constant strength amplitude. Direct evaluation of the ductility capacities of the analyzed cross-sections might not be appropriate to be performed since the piers are loaded through a displacement controlled path. However, even under a controlled displacement loading a comparative evaluation of the ductility capacities between two systems is possible. It is evident from Fig. 9 that the stiffened box cross sectioned pier (No-2), since its strength is dropping at a much higher rate from cycle to cycle compared to the ALT-2 section, is expected to experience smaller ductility than the ALT-2 cross section under seismic loading.

Alternatively, ductility is also related to the area enclosed by a force displacement loop, and by looking in Fig. 10 and Fig. 12 one can conclude that the ductility capacities of the circular cross sectioned pier with cellular stiffeners (ALT-8) and the corrugated cross sectioned pier (ALT-C-8) are higher than the ductility of the circular cross sectioned pier (No-8).

5. Conclusions

New concepts for the design of thin-walled steel columns were introduced in an attempt to mitigate the shortcoming in the response of the conventional designs, stiffened rectangular or box, and circular cross-sections, under dynamic lateral excitations. First FE analysis was employed to calibrate material and geometric models against experimental results available in the literature for stiffened box and circular cross sectioned thin-walled steel bridge piers. The Chaboche material constitutive model which was utilized in this analysis proved adequate to capture the experimental results accurately as showed in the previously presented piers.

The comparisons between the results obtained from the FE analysis of the stiffened box cross sectioned pier (No-2) and the cellular cross sectioned with corrugated stiffeners pier (ALT-2) showed the superior performance of the cellular cross sectioned pier in both the strength and ductility capacities. Similar observations are made when comparing the circular cross sectioned pier (No-8) with both the cellular (ALT-8) and the corrugated (ALT-C-8) cross sectioned piers. Both strength and ductility capacities are superior for the ALT-8 and the ALT-C-8 piers. The main reason for the improved behavior of those innovative cellular and corrugated cross sections is their ability to reduce the buckling potential of their walls and or panels compared to the two conventional cross sections. The cellular form and the corrugations in the cross section of a pier act as vertical stiffeners which result in an increase of the critical buckling strength of the panels and cross section walls. That in turn forces buckling to develop after plastic strains have been developed in the material, thus allowing for full utilization of both the strength and ductility capacities of the cross section. The geometry of the cellular and the corrugated cross sections has an additional beneficial effect. If local buckling takes place in a fold or single corrugation, the abrupt changes in the orientation of the neighboring folds act as barriers and contain buckling within that fold without allowing it to propagate and cause global/wall buckling failure.

The three design alternatives of the conventional thin-walled cross sectioned pier introduced in this paper proved their potential for superior performance in terms of strength and ductility under cyclic lateral loading.

Acknowledgments

The authors gratefully acknowledge the partial support by the National Science Foundation through Grant CMS-0201371, Dr. Peter Chang and Dr. Steven McCabe, Program Directors. The authors are also gratefully acknowledging the two anonymous reviewers for their constructive comments.

References

Ansys Inc. (2004), Ansys V8.1 Users Manual.

Banno, S., Mamaghani, I.H.P., Usami, T. and Mizuno, E. (2000), "Cyclic elastoplastic large deflection analysis of thin steel plates", *J. Eng. Mech.*, ASCE, **124**(4), 363-370.

Bruneau, M., Wilson, J.W. and Tremblay, R. (1996), "Performance of steel bridges during the 1995 Hyogo-ken Nanbu (Kobe, Japan) earthquake", *Canadian J. Civil Eng.*, **23**(3), 678-713.

Chung, R.M., Ballantyne, D.B., Comeau, E., Holzer, T.L., Madrzykowski, D., Schiff, A.J., Stone, W.C., Wilcoski, J., Borcherdt, R.D., Cooper, J.D., Lew, H.S., Moehle, J., Sheng, L.H., Taylor, A.W., Bucker, I., Hayes, J., Leyendecker, E.V., O'Rourke, T., Singh, M.P. and Whitney, M. (1996), "January 17, 1995 Hyogoken-Nanbu (Kobe) earthquake: Performance of structures, lifelines, and fire protection systems", NIST SP 901; ISCCS TR18.

Gao, S., Usami, T. and Ge, H. (1998a), "Ductility of steel short cylinders in compression and bending", *J. Eng. Mech.*, ASCE, **124**(2), 176-183.

Gao, S., Usami, T. and Ge, H. (1998b), "Ductility evaluation of steel bridge piers with pipe sections", *J. Eng. Mech.*, ASCE, **124**(3), 260-267.

Goto, Y., Wang, Q. and Obata, M. (1998), "FEM analysis for hysteretic behavior of thin-walled columns", *J. Struct. Eng.*, ASCE, **124**(11), 1290-1301.

Jiang, L., Goto, Y. and Obata, M. (2002), "Hysteretic modeling of thin-walled circular steel columns under biaxial bending", *J. Struct. Eng.*, ASCE, **128**(3), 319-327.

Kawashima, K., MacRae, G., Hasegawa, K., Ikeuchi, T. and Oshima, K. (1992), "Ductility of steel bridge piers from dynamic loading tests", *Stability and Ductility of Steel Structures under Cyclic Loading*, Y. Fukumoto and G. Lee, eds., CRC Press, Boca Raton, Fla., 149-162.

Kristek, V. and Skaloud, M. (1991), *Advanced Analysis and Design of Plated Structures, Developments in Civil Engineering*, 32, Elsevier, New York.

Lemaitre, J. and Chaboche, J.L. (1990), *Mechanics of Solid Materials*, Cambridge University Press

MacRae, G.A. and Kawashima, K. (2001), "Seismic behavior of hollow stiffened steel bridge columns", *J. Bridge Eng.*, ASCE, **6**(2), 110-119.

Nishikawa, K., Yamamoto, S., Natori, T., Terao, K., Yasunami, H. and Terada, M. (1998), "Retrofitting for seismic upgrading of steel bridge columns", *Eng. Struct.,* **20**(4-6), 540-551.

Uang, C.M., Tsai, K.C. and Bruneau, M. (2000), "Seismic design of steel bridges", Chapter in "The CRC Handbook of Bridge Engineering", CRC Press, Boca Raton, Florida, 39-1, 39-34.

Usami, T. and Ge, H.B. (1998), "Cyclic behavior of thin-walled steel structures-numerical analysis", *Thin Walled Structures*, **32**, 41-80.

Usami, T., Mizutani, Sss., Aoki, T. and Itoh, Y. (1992), "Steel and concrete filled steel compression members under cyclic loading", *Stability and Ductility of Steel Structures under Cyclic Loading*, Y. Fukumoto and G. Lee, eds., CRC Press, Boca Raton, Fla., 123-138.